Applied Catalysis B: Environmental 189 (2016) 1–11

Contents lists available at ScienceDirect

Applied Catalysis B: Environmental

journal homepage: www.elsevier.com/locate/apcatb

A novel sulfur-nitrogen dual doped ordered mesoporous carbon electrocatalyst for efficient oxygen reduction reaction

Tingting Jiang[a], Yi Wang[a,*], Kun Wang[a], Yeru Liang[a], Dingcai Wu[a], Panagiotis Tsiakaras[b,*], Shuqin Song[a,*]

[a] The Key Lab of Low-carbon Chemistry & Energy Conservation of Guangdong Province, Sun Yat-sen University, Guangzhou 510275, China
[b] Laboratory of Alternative Energy Conversion Systems, Department of Mechanical Engineering, School of Engineering, University of Thessaly, Pedion Areos, 38834 Volos, Greece

ARTICLE INFO

Article history:
Received 30 October 2015
Received in revised form 2 February 2016
Accepted 3 February 2016
Available online 6 February 2016

Keywords:
Oxygen reduction reaction
S-N doped ordered mesoporous carbon
Electrocatalytic activity
Methanol tolerance
Stability

ABSTRACT

Despite nitrogen doped carbon (N—C) materials as metal-free electrocatalysts for oxygen reduction reaction (ORR) have shown desirable performance, the state-of-the-art of N—C materials is still far from satisfaction for practical fuel cell applications. In the present work, sulfur (S) and nitrogen (N) dual doped ordered mesoporous carbon (SN-OMC) materials are for the first time successfully obtained by the aid of a convenient method under the same conditions, using polythiophene (PTh) and polypyrrole (PPy) as the precursors, ordered mesoporous silica (SBA-15) as the hard template, and $FeCl_3$ as the catalyst. The preparation conditions of the adopted method are gentle and easy to control and regulate. The experimental results have demonstrated that the obtained materials possess high ordering degree, large specific surface area and adjustable sulfur and nitrogen contents. It is found that the S_1N_5-OMC (the PTh/PPy feeding volume ratio is 0.5:2.5) exhibits excellent ORR electrocatalytic activity in alkaline media with desirable current density, methanol tolerance and long-term stability. Such excellent performance could be attributed to the synergistic effect between S and N, the high density of catalytic sites for ORR provided by high S-N heteroatoms loading, and the excellent mass transfer benefiting from ordered mesoporous pore structure. The present investigation provides a new approach to prepare S and N dual doped mesoporous carbons, which show great potential to be applied as fuel cell cathode electrocatalysts.

1. Introduction

With more and more attention to environmental protection, *polymer electrolyte membrane fuel cells*, which are among the most attractive environmentally friendly energy conversion systems, remain the last decades world-widely an active research topic. *Oxygen reduction reaction* (ORR) is the cathodic reaction in *polymer electrolyte membrane fuel cells* and it takes place mainly through the following two mechanisms:

(i) An efficient four-electron process to produce H_2O in acidic solution or OH^- in alkaline solution;

(ii) A two-electron process which firstly leads to intermediate H_2O_2, and through a further reduction of oxygen leads to H_2O ($O_2 + 2e^- \rightarrow 2O^- + 2e^- \rightarrow 2O^{2-}$).

Obviously, the four-electron process is preferred for a high efficiency output of fuel cell. However, it should be noted that, for both ORR mechanisms, the corresponding kinetics is sluggish [1,2]. Currently, Pt with its efficient catalytic activity and full four-electron process is the most widely used ORR electrocatalyst for *polymer electrolyte membrane fuel cells*. On the other hand, taking into account its high price and its scarce amount, Pt cannot be considered as the most suitable catalyst for commercial applications [3]. Therefore, a great number of investigations have been devoted to the identification of alternative catalysts (active for ORR and cheaper than Pt) to decrease or even avoid the usage of Pt, *i.e.* low Pt or Pt-free catalysts [4–6].

Carbon materials have been adopted as the electrocatalyst support for many years because of their high electrical conductivity,

* Corresponding author.
E-mail addresses: wangyi76@mail.sysu.edu.cn (Y. Wang), tsiak@uth.gr (P. Tsiakaras), stssssq@mail.sysu.edu.cn (S. Song).

http://dx.doi.org/10.1016/j.apcatb.2016.02.009
0926-3373/

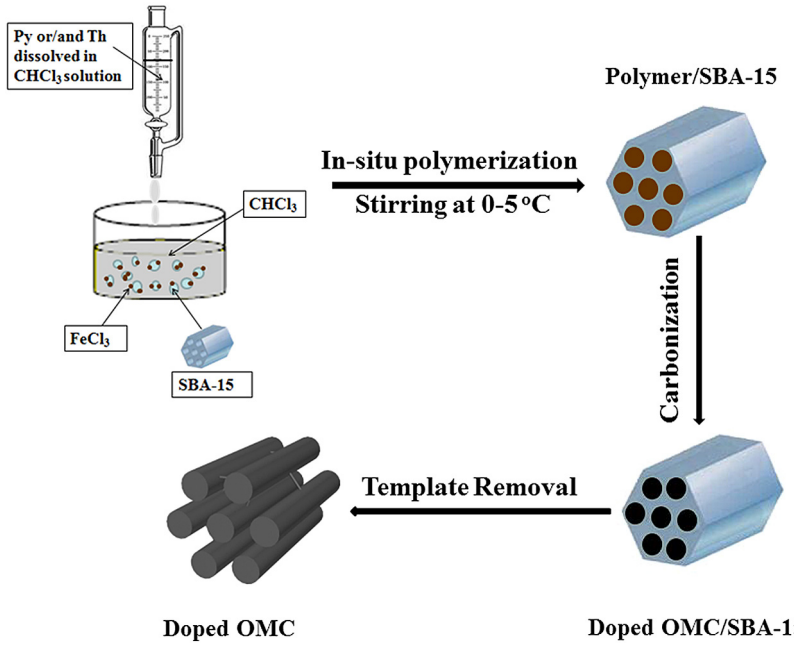

Fig. 1. Schematic scheme of the synthesis process of S or/and N doped ordered mesoporous carbons.

large specific surface area, good decay resistance, low price and easy control of the pore size and morphology. In recent years, different research groups have found that their catalytic performance could be improved by doping proper elements to carbon materials, such as N [7–10], B [11–14], P [15–18], and F [19,20]. This property could be probably due to the new catalytic sites created after the doping with heteroatoms, which polarize spin and charge density distribution of carbon atoms. [21].

Heteroatom-doped carbon materials have been supposed to be of the most potential Pt substitutes for ORR electrocatalysts, exhibiting high efficiency, stability, and low price. According to the previous report [22], there are two main factors affecting the electrocatalytic performance of heteroatom-doped carbon materials. The first factor is the mesoscopic morphology, including the surface area, pore size, and the order degree of the materials. The large surface area always reflects abundant porosity and reaction active sites, which could enhance the ORR catalytic performance. Based on the literature results [23,24], ordered mesoporous

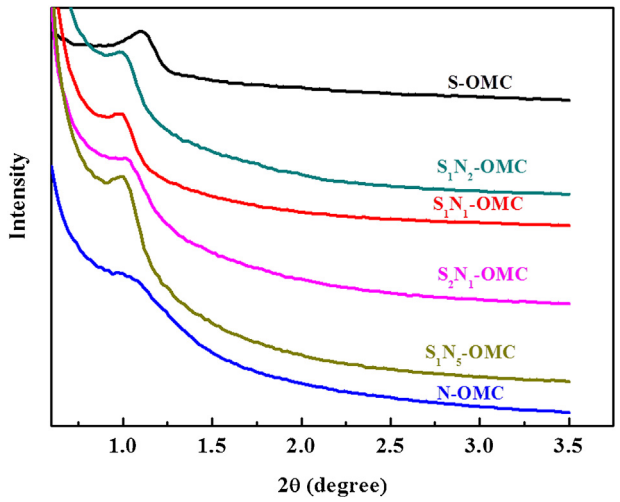

Fig. 2. Small angle X-ray diffraction patterns of all the as-prepared catalysts at a scan rate of 0.3° min^{-1}.

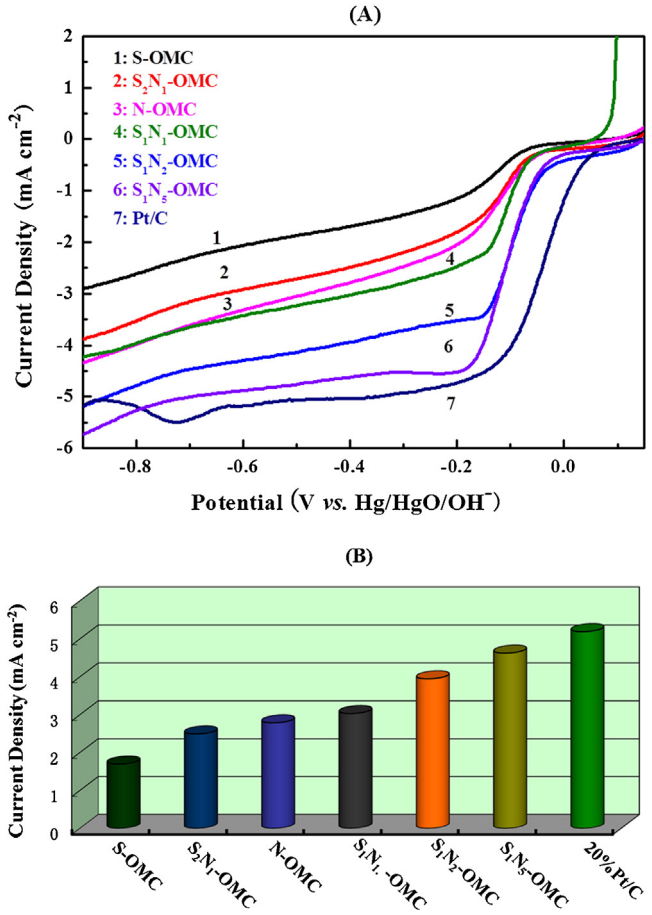

Fig. 3. LSV of all the as-prepared S or/and N doped OMC and the commercial Pt/C (20 wt%) in O_2 saturated 0.1 mol L^{-1} KOH aqueous at a scan rate of 10 mV s^{-1} with a rotation speed of 1600 rpm (A), and their corresponding current density at a given potential of 0.4 V (B).

carbon materials are suitable for ORR because of their relatively large surface area, proper pore size (2–50 nm) and regular pore structure, which favor mass transfer during the reaction process. The second factor is the microscopic structure, mainly involving the structure control at an atomic level. In this aspect, increasing the heteroatom content and tuning the species of the doped atoms and heteroatom bonding modes [25–27], has been verified to be a valid way for the improvement of ORR activity. Many researchers paid more attention to nitrogen (N) atom doping because of its excellent performance; however its state-of-the-art performance has not satisfied some ORR requirements yet. Among the elements of periodic table, sulfur (S) is on the bottom right of N, which is also confirmed to exhibit some beneficial effect on the ORR activity of carbon materials [21,29–31]. The excellent ORR activity of N-doped materials may be attributed to the larger electronegativity of N with respect to C atoms, and the creating of positive charge density on the adjacent C atoms. Unlike N, S, which have similar electronegativity with carbon, is more likely beneficial from its long S—C bonds, which are predominately at the edge or the defect sites, and polarize spin distribution of carbon atoms [21]. The dual heteroatoms doped by both S and N is expected to enhance the ORR activity of OMCs more than single N doping does, mostly due to the synergistic effect. Recently, some works have been devoted to the synthesis of S and N dual doped carbon materials, such as honeysuckles-derived S and N doped porous carbon [32], S and N doped multiwalled carbon nanotubes [33], and S and N doped graphene [34], which demonstrated relatively good ORR catalytic performance. However, the synthetic method and the way for adjusting the S/N content ratio still consist of the main barriers.

Herein we report a practical one-step synthetic method for a series of S or/and N mono and dual doped ordered mesoporous carbon materials with easy adjusting of N and S content and we discuss their synergistic effects in the dual doping case. More precisely, in the present investigation, ordered mesoporous silica (SBA-15) was used as the hard template, and thiophene or/and pyrrole as monomers were *in-situ* polymerized. Thiophene and pyrrole are similar in many aspects such as the molecular structure, the state of matter and density, which indicates that a uniform condition could be adopted for the further polymerization. The main difference is the S atom in thiophene instead of N in pyrrole, which can provide the opportunity for synergy phenomena. The as-prepared catalysts were characterized by *X-ray diffraction* (XRD), *transmission electron microscopy* (TEM), *scanning electron microscopy* (SEM), *X-ray photoelectron spectroscopy* (XPS) and *elemental analysis* (EA). The electrocatalytic activities for ORR, methanol tolerance and stability were measured by *cyclic voltammetry* (CV) and *linear sweep voltam-*

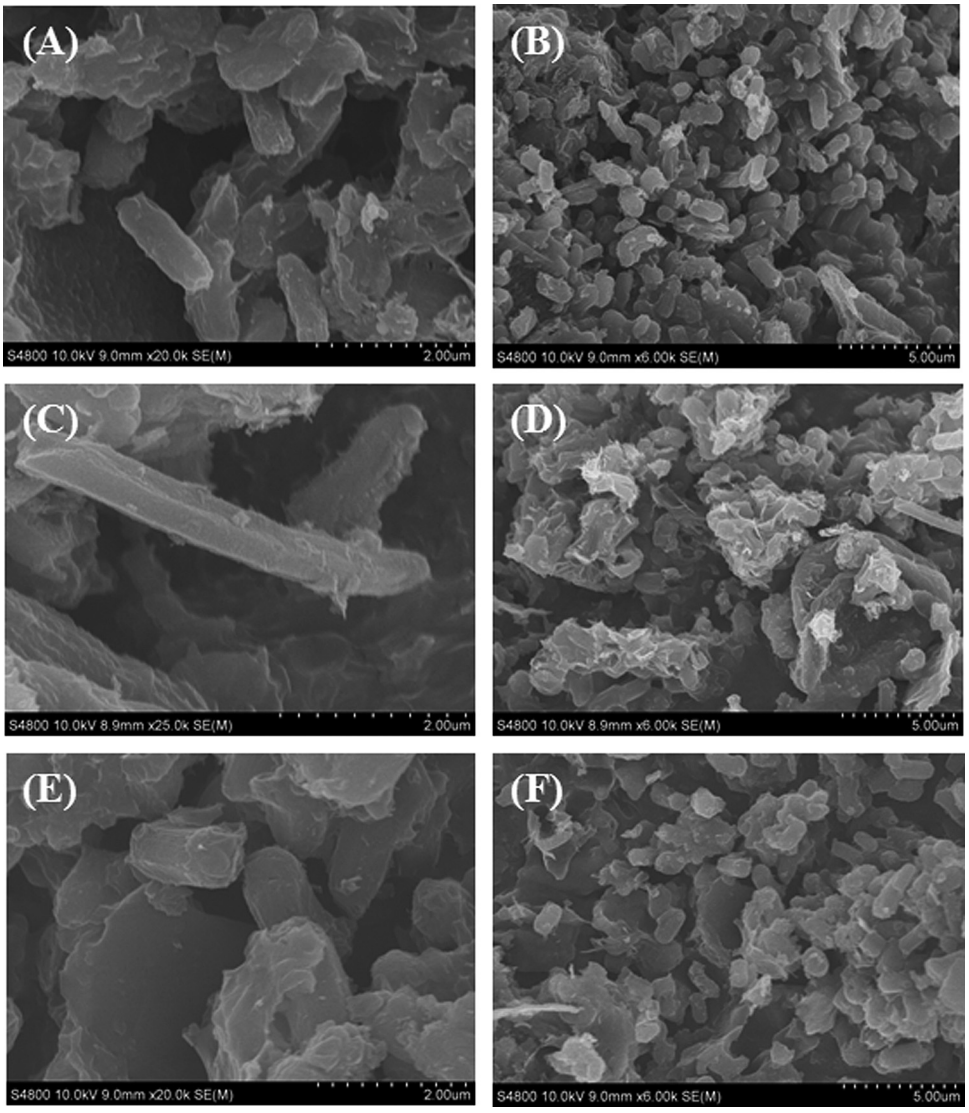

Fig. 4. SEM images of S-OMC (A and B), N-OMC (C and D), and S_1N_5-OMC (E and F).

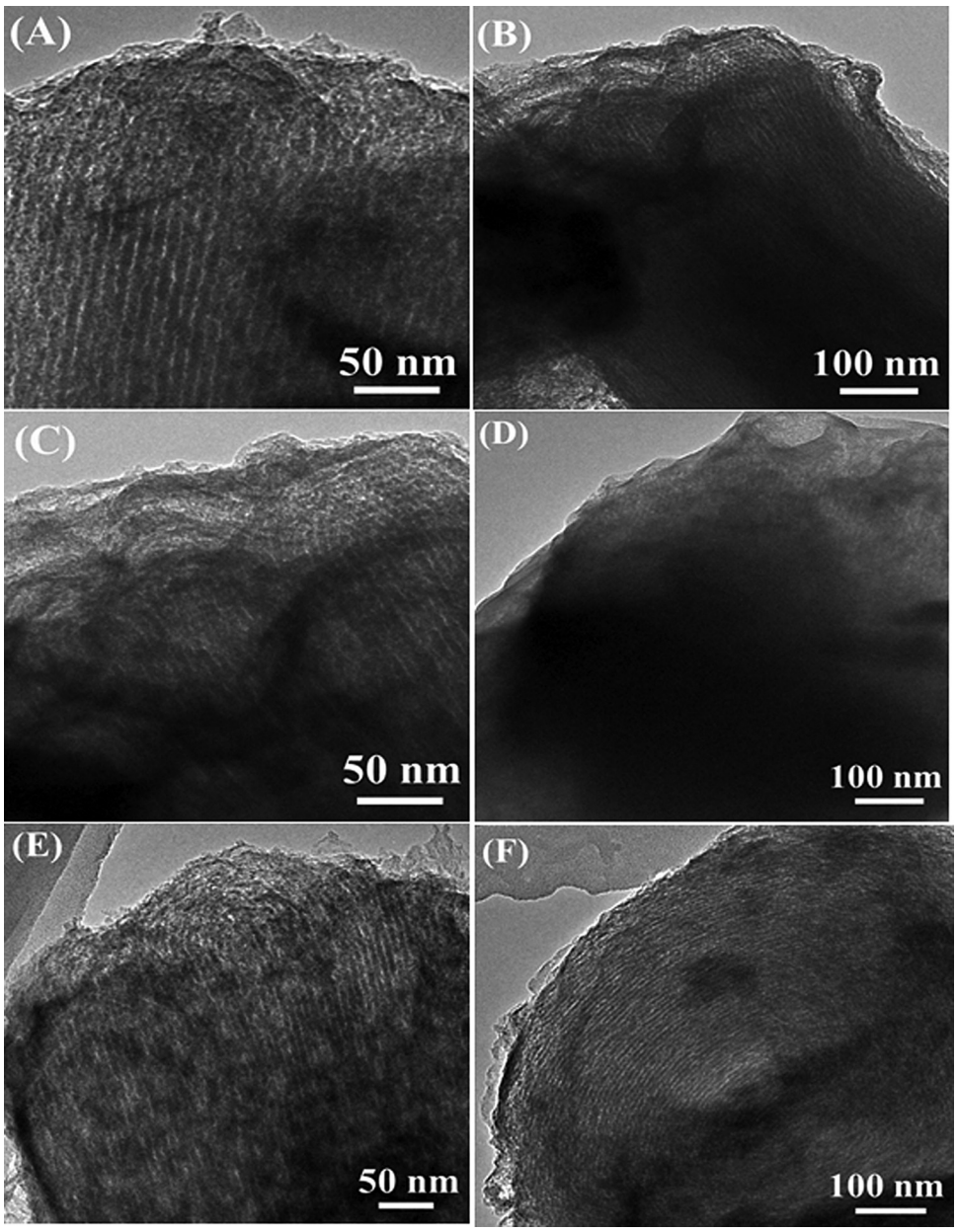

Fig. 5. TEM images of S-OMC (A and B), N-OMC (C and D), and S_1N_5-OMC (E and F).

metry (LSV) using *rotating ring-disk electrode* (RRDE) techniques in alkaline media.

2. Experimental

2.1. Ordered mesoporous silica (SBA-15) synthesis

2.1.1. Fabrication of SBA-15 hard template

SBA-15 was synthesized according to a previous report [35]. Briefly, pluronic P123 (EO_{20}-PO_{70}-EO_{20}, MW ~ 5800, Aladdin®), tetraethyl orthosilicate ($Si(OC_2H_5)_4$, Aladdin®, denoted as TEOS), HCl (37 wt%) and H_2O were well mixed with the ratio of 1.00 g: 1.73 mL: 0.46 mL: 18.20 mL. After vigorous stirring of P123, H_2O and HCl, TEOS was added, and then the mixture was left under vigorous stirring at 35 °C for 24 h. The mixture was subsequently treated at 100 °C for another 24 h under the static station. The white product was obtained by filtration, washed with distilled water, dried in vacuum, and finally calcined at 550 °C for 6–10 h in air.

2.2. S or/and N doped ordered mesoporous carbons (OMCs) synthesis

The synthesis process of S or/and N doped ordered mesoporous carbons is schematically shown in Fig. 1. Firstly, 1.00 g of SBA-15 and 24.30 g anhydrous ferric chloride as the catalyst for polymerization were uniformly dispersed in chloroform by vigorous stirring and ultrasonication. Then thiophene (C_4H_4S, Aladdin®, denoted as Th) or/and pyrrole (C_4H_5N, Aladdin®, denoted as Py) as monomers, which were beforehand dissolved in 50.0 mL chloroform, were added into the mixture drop by drop under vigorous stirring for polymerization at 0–5 °C for about 8 h into PTh or/and PPy. After that, the mixture was washed by 100.0 mL chloroform for 3 times and then soaked in 1.0 mol L^{-1} HCl aqueous solution for 2 h to remove the residual monomer and Fe catalyst, and then washed by deionized water. The product was dried in a vacuum oven at 60 °C for 12 h. The resulted powder was pyrolysed at 800 °C in a tube furnace for 3 h, at a heating rate of 1 °C min^{-1} from room tem-

Table 1
Elemental analysis results of all the as-prepared catalysts.

Samples	Weight (mg)	C (wt%)	H (wt%)	N (wt%)	S (wt%)
S-OMC	1.5630	77.58	1.564	–	13.57
S_2N_1-OMC	2.0300	78.60	1.536	1.23	8.775
S_1N_1-OMC	1.5610	73.87	1.264	2.90	10.45
S_1N_2-OMC	2.1000	70.97	1.514	3.45	7.113
S_1N_5-OMC	2.0550	72.48	1.763	5.72	5.641
N-OMC	1.0690	72.47	1.745	9.43	–

perature to 600 °C and then 5 °C min^{-1} to 800 °C in a flowing N_2 atmosphere. After etching the SBA-15 template by HF, the doped carbon materials were collected by washing and drying.

Different S/N content materials were prepared by simply adjusting the feeding volume ratio between thiophene and pyrrole (0:3, 0.5:2.5, 1:2, 1:1, 2:1, and 3:0). According to the above feeding volume ratio, the corresponding samples were denoted as S-OMC, S_1N_5-OMC, S_1N_2-OMC, S_1N_1-OMC, S_2N_1-OMC, and N-OMC, respectively.

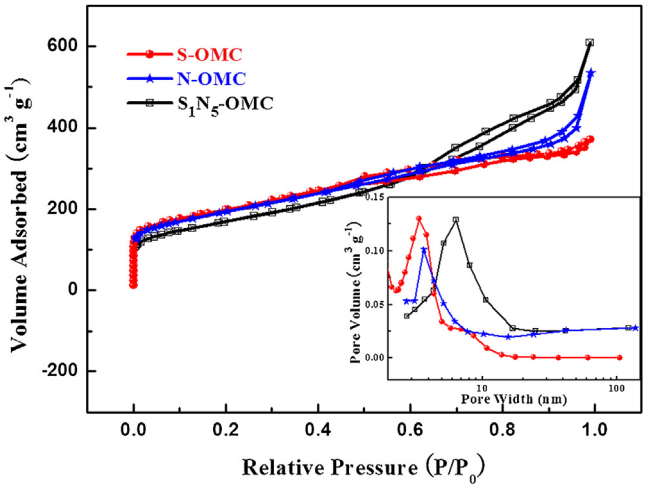

Fig. 6. N_2 adsorption-desorption isotherms of S_1N_5-OMC, N-OMC and S-OMC (the inset shows their BJH pore size distributions).

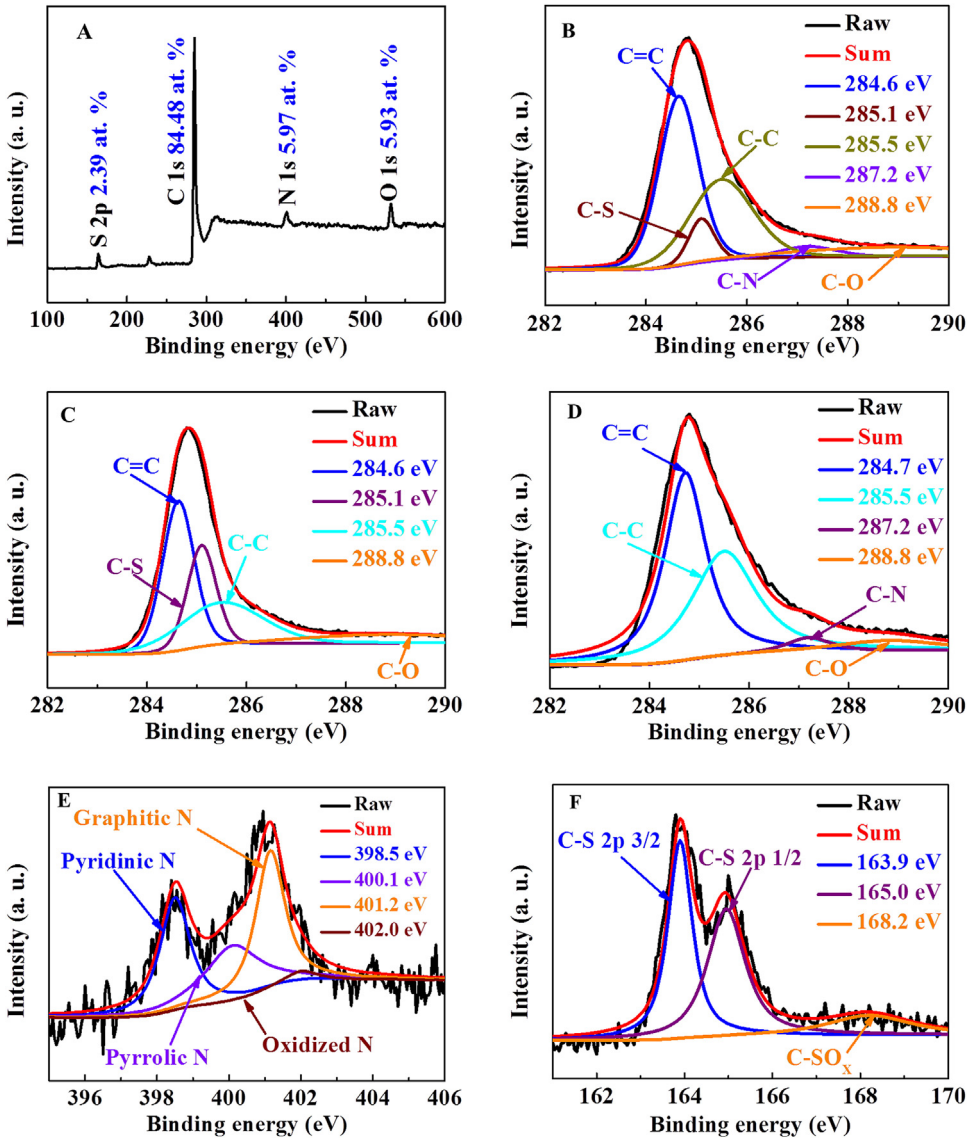

Fig. 7. XPS survey of the S_1N_5-OMC (A); the high-resolution C_{1s} XPS spectrum of S_1N_5-OMC (B), S-OMC (C), N-OMC (D); the high-resolution N_{1s} XPS spectrum of S_1N_5-OMC (E); the high-resolution S_{2p} XPS spectrum of S_1N_5-OMC (F).

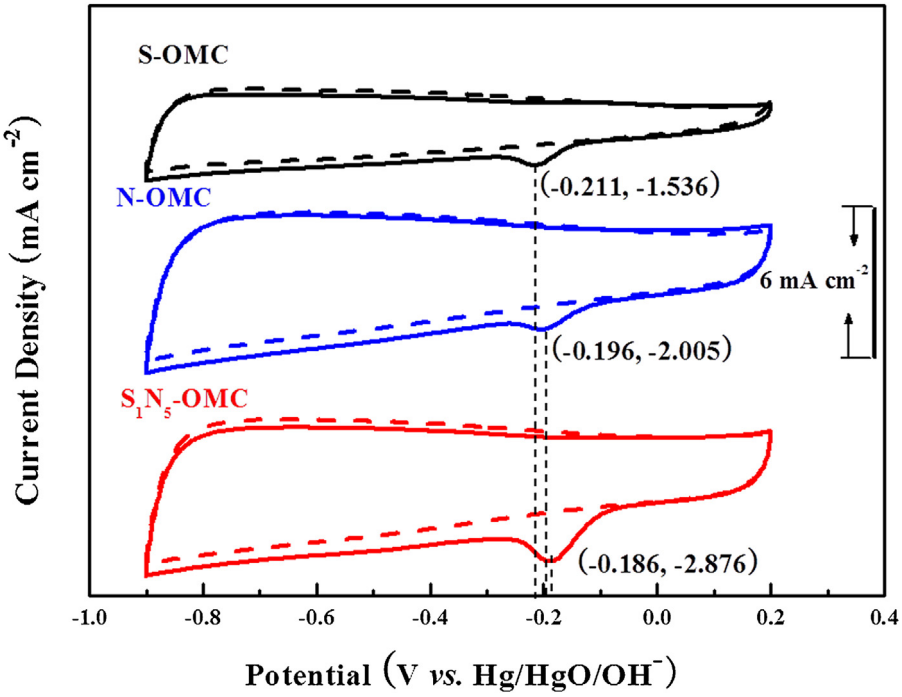

Fig. 8. CV curves of S-OMC, N-OMC, and S_1N_5-OMC in N_2- (dash line) and O_2- (solid line) saturated 0.1 mol L^{-1} KOH aqueous solution at a scan rate of 20 mV s^{-1}.

2.3. Physico-chemical characterization

The structure and morphology were characterized by *small angle X-ray powder diffraction* (SAXD) (Rigaku Co., Japan) with Cu Kα radiation (40 kV, 26 mA), SEM (JSM-6330F, Japan) and TEM (JEOL TEM-2010, HR). The nitrogen adsorption/desorption data were obtained by using Micromeritics ASAP2020. Before the measurements, the materials were dried at 250 °C for 8 h in vacuum. The specific surface area was calculated using the Brunauer–Emmett–Teller (BET) formula. XPS measurements were performed on a VG Scientific ESCALAB250 using Al Kα radiation (1486.6 eV). Spectrograms were analyzed with Xpspeak41 software. EA was carried out by the aid of Element Analyzer system GmbH Vario EL.

2.4. Electrochemical analysis

All the electrochemical measurements were carried out using an AUT84480 instrument in a three-electrode system coupled with a PINE RRDE (from Pine Instruments Co., Ltd., USA). Hg/HgO electrode (0.1 mol L^{-1} KOH), which potential was 0.164 V (*vs.* NHE (normal hydrogen electrode)), was used as the reference electrode. Platinum foil (2.0 cm × 1.0 cm) was adopted as the counter electrode. The working electrode was prepared by dispersing 10.0 mg of the as-prepared catalyst powder in 350.0 μL ethanol and 95.0 μL Nafion® solution (5.0 wt% Dupont Company). The suspension was sonicated for about 30 min in an ice-water bath. Then, 7.0 μL of this ink was transferred onto the surface of the glassy carbon electrode with an area of 0.247 cm^2, and then the electrode was dried in air. For the sake of comparison, the working electrode, also with the commercial Pt/C (20 wt Pt%, Johnson Matthey Corp.) as the catalyst, was prepared with 10.0 mg of Pt/C in 1.80 mL ethanol and 0.20 mL Nafion solution. Then, 10.0 μL of this ink was transferred onto the surface of the glassy carbon electrode. The ORR performance of the catalysts was first evaluated by the LSV curves in O_2-saturated aqueous solution of 0.1 mol L^{-1} KOH with a scan rate of 10 mV s^{-1} under the rotation speed of 1600 rpm. The ring electrode potential was set as 0.5 V [9]. CV in O_2-free and O_2-saturated solution with 0.1 mol L^{-1} KOH at a scan rate of 20 mV s^{-1} were also obtained to check the ORR performance. The methanol tolerance was tested by CV with or without methanol. In order to evaluate the stability of the catalyst, accelerating degradation CV was also performed for 1500 cycles from 0.2 V to −0.9 V at a scan rate of 20 mV s^{-1}, and then the LSV curves were obtained to evaluate the stability. Without specification, all the potentials are referred to the Hg/HgO (0.1 mol L^{-1} KOH) reference electrode.

3. Results and discussions

Fig. 2 shows the small-angle XRD patterns of all the as-prepared carbon based composite materials. All the samples show a 2θ peak at *ca.* 1°, which stands for diffraction peak (1 0) of 2D hexagonal structure, indicating an ordered mesoporous frame derived from SBA-15 template [36,37]. This phenomenon indicates that thiophene and pyrrole have been polymerized inside the SBA-15 pore channels, and reserves the duplicate structure of SBA-15 after the processes of the polymerization and etching of the templates.

The electrocatalytic activities of all the samples in alkaline media were preliminary assessed by LSV curves in a three-electrode system. From the curves depicted in Fig. 3A, the mono S doped OMC (S-OMC) exhibits the worst ORR performance, no matter in terms of limited current density or in terms of onset potential. Once N precursor (Py) is introduced, the corresponding ORR activity is significantly and monotonously increased. Moreover, in the case of higher Th/Py volume ratio (2:1), its ORR activity is still lower than that on the mono N doped OMC (N-OMC). Since Th/Py volume ratio of 1:1, the S and N dual doped OMC starts to present better ORR performance than mono N doped OMC. Obviously, mono N doping can provide more beneficial effect on the OMC's activity towards ORR than mono S doping. The dual doping of S and N can take advantage of the synergetic function of the coupling interaction between S and N heteroatoms with the optimized S/N ratio [38], which makes the dual doped catalysts exceed the mono doped ones in terms of ORR performance. The effect of N and S content in mono and dual doped OMC on ORR activity can be clearly seen from Fig. 3B, in which S_1N_5-OMC exhibits the best ORR electrocatalytic activity among all

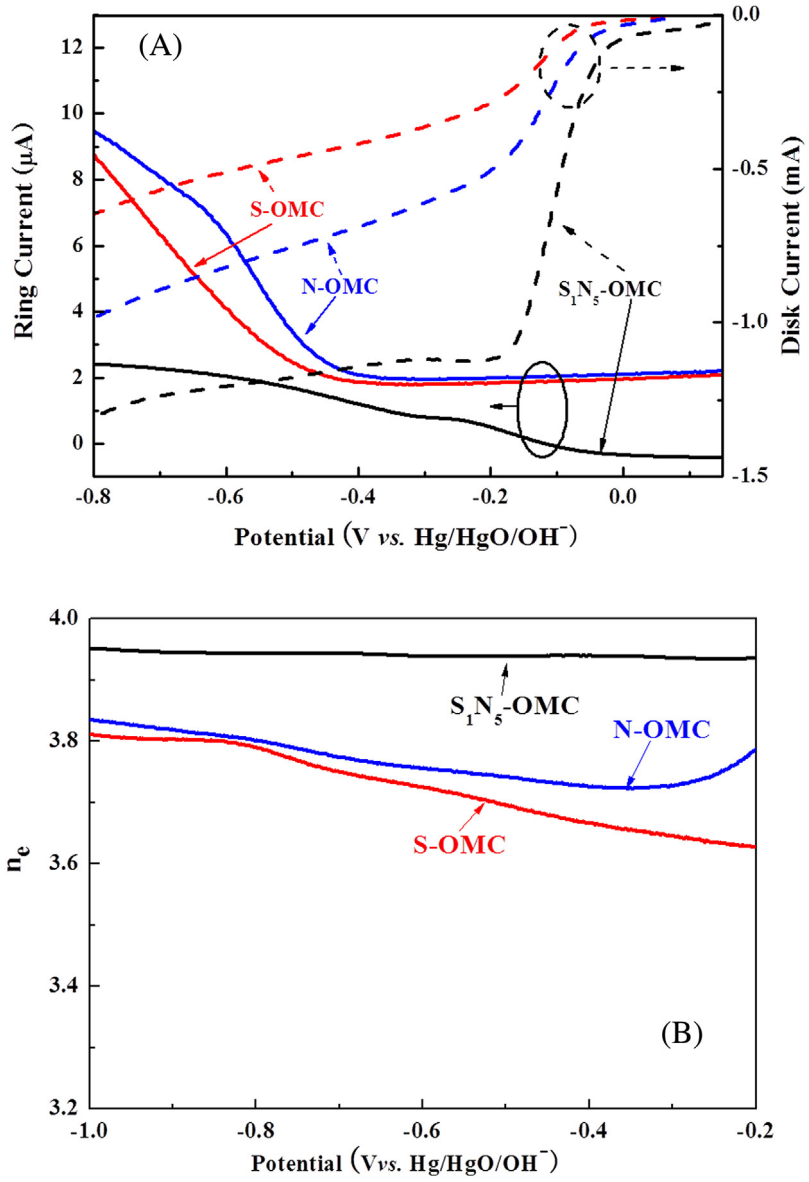

Fig. 9. RRDE (A) and electron-transfer numbers involved in ORR process (B) of S-OMC, N-OMC and S_1N_5-OMC in O_2 saturated 0.1 mol L^{-1} KOH aqueous solution at a scan rate of 10 mV s^{-1} with a rotation speed of 1600 rpm.

the investigated OMC based composite materials. Moreover, S_1N_5-OMC exhibits comparable ORR activity to the commercial Pt/C, in terms of current density but a little disadvantage in the ORR onset potential.

In order to explore the synergetic effect between S and N heteroatoms, further physico-chemical characterizations for S-OMC, N-OMC and S_1N_5-OMC were carried out. From the typical SEM images of S_1N_5-OMC (Figs. 4A and 4B), some rodlike particles are observed, with a hexagonal structure and thickness of about 0.5 μm, typical of SBA-15 structure [39]. Besides the rods, there are some plate-like structures, which could be derived from the inevitable polymer that was not filled into the templates. Almost the same structure can be also seen in the mono doped samples (S-OMC in Figs. 4C and 4D; N-OMC in Figs. 4E and 4F), indicating a very good duplicate of SBA-15 template and almost the same structure of these three materials. Furthermore, the parallel channels in the TEM images (Fig. 5) again verify the ordered structure of S-OMC, N-OMC, and S_1N_5-OMC, which is in agreement with the results of small angle XRD patterns.

In order to investigate the pore structure of the as-prepared samples, the nitrogen adsorption-desorption isotherms were performed and the results are shown in Fig. 6. For both of mono doped carbons and S_1N_5-OMC, typical IV nitrogen adsorption/desorption isotherms are observed, with distinct H1 hysteretic loop, which indicates the mesoporous structure including capillary condensation. The pore size distribution (inset of Fig. 6), investigated by the BJH method, clearly displays an obvious peak at about 6.2 nm for S_1N_5-OMC, which is due to the etching of SBA-15 template. The BET surface area of the dual doped material is found to be 601.7 m^2 g^{-1}. The mono doped S-OMC and N-OMC shows typical mesoporous structure with an average pore size between 4.0–5.0 nm (inset of Fig. 6). It can also be seen that their corresponding BET surface areas are 621.7 m^2 g^{-1} for S-OMC and 686.7 m^2 g^{-1} for N-OMC, respectively. The similar pore size and surface area values among S-OMC, N-OMC, and S_1N_5-OMC suggest that the superiority of S_1N_5-OMC in ORR activity could be attributed not to structure reasons, but to the synergetic effect between N and S.

For the N or/and S contents measurement and for the chemical bonds formed among the elements, the EA and XPS results

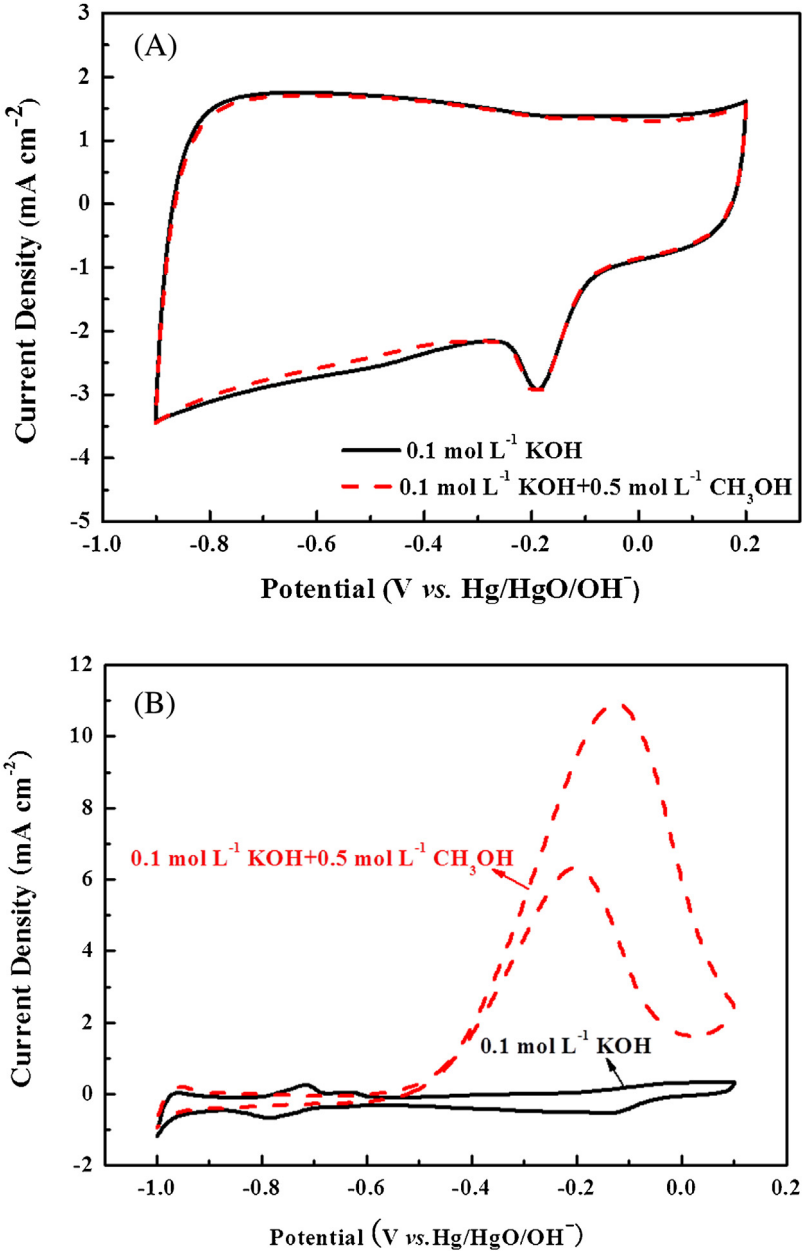

Fig. 10. CV curves of S_1N_5-OMC in O_2 saturated 0.1 mol L^{-1} KOH and 0.5 mol L^{-1} CH_3OH + 0.1 mol L^{-1} KOH (A), and commercial Pt/C (20 wt.%) in O_2 saturated 0.1 mol L^{-1} KOH and 0.1 mol L^{-1} KOH + 0.5 mol L^{-1} CH_3OH (B).

were respectively obtained and analyzed. The N/S contents of all samples are given in Table 1. As it can be seen, for the S-OMC, the S contents reaches the very high value of 13.57 wt%, while for the N-OMC the N content is as high as 9.43 wt%. For the S and N dual doped OMCs, the N and S relative contents increase as the feeding ratio between Py and Th increases. On the other hand, the S/N weight ratios do not match the feeding ratio so well, probably because PPy is easier decomposed than PTh in the same pyrolysis system. The XPS results showed the surface atomic percentages of C (84.48 at.%), O (5.93 at.%), N (5.97 at.%), S (2.39 at.%) for the S_1N_5-OMC catalyst (Fig. 7A). This result confirms that N and S atoms have been successfully incorporated into the carbon framework. High resolution XPS was performed to further investigate the bonding configurations. As shown in Fig. 7B, the C1s spectrum of the S_1N_5-OMC displays an asymmetric shape with the peak energy of 284.79 eV and the peak could be deconvoluted into five C species, corresponding to C═C (284.6 eV), C-S (285.1 eV), C—C (285.5 eV), C—N (287.2 eV), and C—O (288.8 eV) [28]. However, the C1s spectra of the S-OMC and N-OMC could be separately deconvoluted into four C species, corresponding to C═C (284.6 eV), C—S (285.1 eV), C—C (285.5 eV), C—O (288.8 eV) for S-OMC and C═C (284.6 eV), C—C (285.5 eV), C—N (287.2 eV), C—O (288.8 eV) for N-OMC, respectively (Figs. 7C and 7D). These results prove the synergistic effect between C—N and C—S for the N and S dual doped OMC, which could improve the ORR performance. The high resolution N1s spectrum of the S_1N_5-OMC (Fig. 7E) can be assigned into three N species, corresponding to pyridinic-N (398.5 eV), pyrrolic-N (400.1 eV), graphitic-N (401.2 eV) and oxidized N (402.0 eV), respectively, further confirming four types of N species in the carbon framework. Remarkably, the pyridinic-N, pyrrolic-N and graphitic-N are recognized as ORR-active species. Similarly, a detailed scan of S2p spectrum (Fig. 7F) can be fitted into three peaks, in which the two peaks at 163.9 eV and 165.0 eV are assigned to thiophene-S (—C—S—C—) owing to the spin-orbit

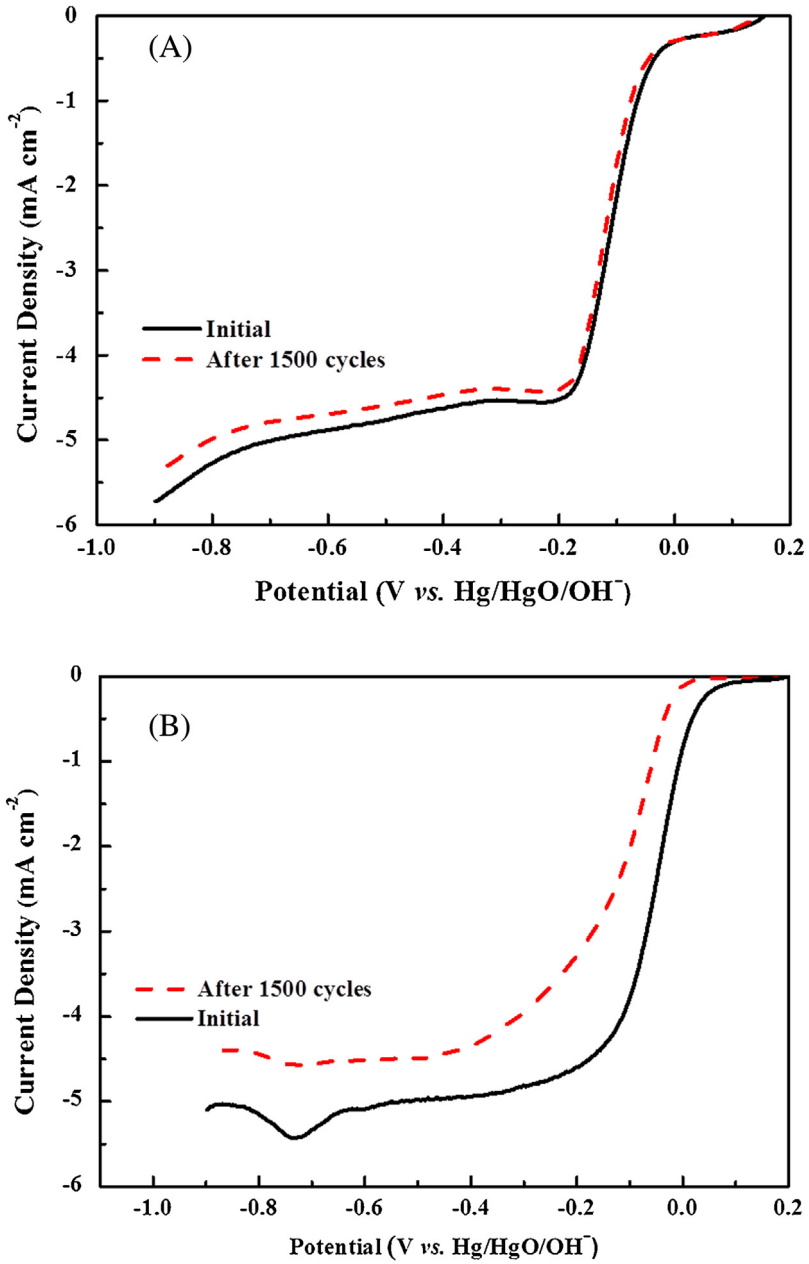

Fig. 11. LSV curves of S_1N_5-OMC (A) and commercial Pt/C (20 wt%) (B) before and after 1500CV cycles in the potential range from 0.2 V to −0.9 V in O_2 saturated 0.1 mol L^{-1} KOH aqueous at a scan rate of 20 mV s^{-1}.

coupling, and the intense peak at 168.2 eV corresponds to the oxidizedS (—C-SOX-C—). The thiophene-S indicates the incorporated S atoms are mainly bonded with two C atoms at the edges and defects of ordered mesoporous carbon, which are chemically active for ORR [28].

As the attractive potential candidate for ORR electrocatalyst, the corresponding ORR activity and selectivity for four-electron process, tolerance to methanol, and stability of S_1N_5-OMC were further investigated. Firstly, the electrocatalytic activity of S_1N_5-OMC towards ORR was assessed by the aid of CV in O_2-free and O_2-saturated solution in 0.1 mol L^{-1} KOH at a scan rate of 20 mV s^{-1} and the results are shown in Fig. 8. In O_2-free solution, S_1N_5-OMC exhibits almost featureless CV, as a result of the typical supercapacitance effect on mesoporous carbon materials. In contrast, when the electrolyte solution is saturated with O_2, a well-defined characteristic ORR peak, centered at about −0.186 V, appears. Under the same conditions, S-OMC and N-OMC show the corresponding ORR peak at −0.211 and −0.196 V respectively, which are both more negative than that observed on S_1N_5-OMC. Moreover, the peak current density of ORR on S_1N_5-OMC is higher than those on both N-OMC and S-OMC. These results further verify that the S and N dual doping can provide synergetic effect on improving ORR performance, which is in agreement with the results shown above (Fig. 3). For the ORR, the four-electron selectivity is crucial for high fuel cell efficiency. Consequently, it is necessary to further gain the insight into the ORR mechanism on the as-prepared samples. For this reason, by the aid of a RRDE, the LSV curves of S-OMC, N-OMC and S_1N_5-OMC were recorded in 0.1 mol L^{-1} KOH saturated with O_2. As it can be seen in Fig. 9A, where the disk electrode results are reported in terms of both onset potential and current density of ORR, S_1N_5-OMC exhibits superior performance to mono doped OMC. For the ring electrode, the much lower ring current measured on S_1N_5-OMC, than that

on both N-OMC and S-OMC, suggests that the four-electron pathway of ORR prevails on S_1N_5-OMC. The transferred electron number (n_e) per oxygen molecule involved in ORR process was calculated through Eq. (1) and it was found to be very close to 4.0 in all the investigated potential range.

$$n_e = \frac{4I_d}{(I_d + I_r/N)} \quad (1)$$

where N = 0.37 is the collection efficiency, I_d the faradic disk current and I_r the faradic ring current.

Based on the results of Fig. 9A, the calculated results of the transferred electron number (n_e) of ORR on different catalysts in the investigated potential range are reported in Fig. 9B. It can be clearly seen that n_e on S_1N_5-OMC is bigger than that on mono heteroatom doped OMC. The n_e on S_1N_5-OMC ranges from 3.93 to 3.95, very close to 4.0, indicating that S_1N_5-OMC favors a four-electron ORR process. On the other hand, the n_e on S-OMC and N-OMC are found to be in the range of 3.63–3.81 and 3.72–3.83, respectively. Together with the bigger ring current shown in Fig. 9A, one can deduce that the mono doped OMCs also mainly favor the four-electron process, however in some extent 2-electron ORR process still occurs.

It is known that in the case of *direct methanol fuel cells* (DMFCs), methanol can permeate from the anode to the cathode, as called methanol crossover. The crossovered methanol would seriously damage DMFC efficiency, which can be dramatically reduced by more than 50% at low current densities [40]. Consequently, for a new candidate electrocatalyst for the ORR in DMFCs, it is also important to check its corresponding catalytic selectivity towards ORR in presence of methanol, *i.e.* methanol tolerance. To this purpose, S_1N_5-OMC was subjected to the 0.1 mol L^{-1} KOH solution containing both saturated O_2 and 0.5 mol L^{-1} methanol or only saturated O_2 and the results are shown in Fig. 10A. As it can be distinguished, the presence of methanol has almost no effect on the ORR electrocatalytic performance of S_1N_5-OMC, indicating both high selectivity towards ORR and high methanol tolerance of S_1N_5-OMC. On the other hand, it can be seen that in the case of commercial Pt/C, there is an obvious peak due to methanol oxidation. In this way a mixed potential is generated causing the decrease of ORR performance. The best ORR performance electrocatalysts should simultaneously possess high activity and long-term stability.

Electrochemical accelerating testing through cyclic voltammetry is a commonly used way to check the stability of the catalyst. The potential cycling was carried out in the potential range from 0.2 V to −0.9 V at a scan rate of 20 mV s^{-1} in O_2 saturated 0.1 mol L^{-1} KOH solution. The corresponding LSV results of ORR, shown in Fig. 11A, were obtained before and after potential cycling on S_1N_5-OMC and the commercial Pt/C. As it can be seen on S_1N_5-OMC there is almost no decay in ORR performance in terms of both onset potential and current density, while on the commercial Pt/C (Fig. 11B), after potential cycling the ORR onset potential is positively shifted by about 70 mV and the current density is about 0.5 mA cm^{-2}, lower than the initial value. Obviously, S_1N_5-OMC exhibits comparable but a little less ORR activity to the commercial Pt/C, and even better methanol tolerance and long-term stability than Pt/C.

4. Conclusion

In summary, S or/and N mono and dual doped ordered mesoporous carbons have been successfully fabricated through a convenient, economical, and scalable route.

The N to S ratio in the S_xN_y-OMC catalysts can be easily regulated and controlled by simply adjusting the feeding ratio of the precursors of thiophene and pyrrole.

The mono N doping exhibits more beneficial effect on the OMC's activity towards ORR than mono S doping. Moreover, the S and N dual doped catalysts exceed the mono doped ones in terms of ORR performance with the optimized S/N atomic ratio in the dual doped OMC.

S_1N_5-OMC shows the best ORR performance in all of the investigated samples. S_1N_5-OMC possesses desirable ORR current density, even a little lower than the commercial Pt/C, but exhibits higher methanol tolerance and longer-term stability than the commercial Pt/C in alkaline medium.

The synergetic effect of N and S dual doping and the ordered pore structure demonstrated in the present investigation could be instructive for other metal-free economical and efficient ORR catalysts.

Acknowledgements

The authors are grateful to the Sino-Greek Science and Technology Cooperation Project (2013DFG62590), to the National Natural Science Foundation of China (Grant No. 21576299, 21576300, 21276290), and to the Guangdong Province Nature Science Foundation (2014A030313150) for financial support. Prof. Tsiakaras is also grateful to the Ministry of Education and Science of the Russian Federation (Mega-Grant, contract no. 14.Z50.31.0001) for funding. Specials thanks to Prof. Wenjie Mai from Jinan University for his professional suggestions and modifications.

References

[1] J.M. Noël, A. Latus, C. Lagrost, E. Volanschi, P. Hapiot, J. Am. Chem. Soc. 134 (2012) 2835–2841.
[2] C.C.M. Neumann, E. Laborda, K. Tschulik, K.R. Ward, R.G. Compton, Nano Res. 6 (2013) 511–524.
[3] T.T. Jiang, L.L. Yan, Y.Z. Meng, M. Xiao, Z.R. Wu, P. Tsiakaras, S.Q. Song, Appl. Catal. B: Environ. 162 (2015) 275–281.
[4] A. Brouzgou, S.Q. Song, P. Tsiakaras, Appl. Catal. B: Environ. 127 (2012) 371–388.
[5] Y. Wang, S. Song, V. Maragou, P.K. Shen, P. Tsiakaras, Appl. Catal. B: Environ. 89 (2009) 223–228.
[6] S. Song, Y. Wang, P. Tsiakaras, P.K. Shen, Appl. Catal. B: Environ. 78 (2008) 381–387.
[7] K. Wan, G.F. Long, M.Y. Liu, L. Du, Z.X. Liang, P. Tsiakaras, Appl. Catal. B: Environ. 165 (2015) 566–571.
[8] J. Wang, G.X. Wang, S. Miao, X.L. Jiang, J.Y. Li, X.H. Bao, Carbon 75 (2014) 381–389.
[9] K.P. Gong, F. Du, Z.H. Xia, D. Michael, L.M. Dai, Science 5915 (2009) 760–764.
[10] H.P. Cong, P. Wang, M. Gong, S.H. Yu, Nano Energy 3 (2014) 55–63.
[11] Z. Sheng, H. Gao, W. Bao, F. Wang, X. Xia, J. Mater. Chem. 22 (2012) 390–395.
[12] Y. Zhao, L.J. Yang, S. Chen, X.Z. Wang, Y.W. Ma, Q. Wu, Y.F. Jiang, W.J. Qian, Z. Hu, J. Am. Chem. Soc. 135 (2013) 1201–1204.
[13] L. Ferrighi, M. Datteo, C.D. Valentin, J. Phys. Chem. 118 (2014) 223–230.
[14] J.T. Jin, F.P. Pan, L.H. Jiang, X.G. Fu, A.M. Liang, Z.Y. Wei, J.Y. Zhang, G.Q. Sun, ACS Nano 4 (2014) 3313–3321.
[15] D.S. Yang, D. Bhattacharjya, M.Y. Song, J.S. Yu, Carbon 67 (2014) 736–743.
[16] R. Li, Z.D. Wei, X.L. Gou, W. Xu, RSC Adv. 3 (2013) 9978–9984.
[17] U.B. Nasini, V.G. Bairi, S.K. Ramasahayam, S.E. Bourdo, T. Viswanathan, A.U. Shaikh, ChemElectroChem 1 (2014) 573–579.
[18] J. Wu, Z.R. Yang, Z.J. Wang, Q.J. Sun, R.Z. Yang, Electrochem. Commun. 42 (2014) 46–49.
[19] X.J. Sun, Y.W. Zhang, P. Song, J. Pan, L. Zhuang, W.L. Xu, W. Xing, ACS Catal. 3 (2013) 1726–1729.
[20] H.W. Wang, A.G. Kong, Mater. Lett. 136 (2014) 384–387.
[21] Z. Yang, Z. Yao, G.F. Li, G.Y. Fang, H.G. Nie, Z. Liu, X.M. Zhou, X.A. Chen, S.M. Huang, ACS Nano 6 (2012) 205–211.
[22] Z. Liu, H.G. Nie, Z. Yang, J. Zhang, Z.P. Jin, Y.Q. Lu, Z.B. Xiao, S.M. Huang, Nanoscale 5 (2013) 3283–3288.
[23] W. Yang, T.P. Fellinger, M. Antonietti, J. Am. Chem. Soc. 133 (2011) 206–209.
[24] P.H. Matter, L. Zhang, U.S. Ozkan, J. Catal. 239 (2006) 83–96.
[25] Y. Wang, Y.Y. Shao, D.W. Matson, J.H. Li, Y.H. Lin, ACS Nano 4 (2010) 1790–1798.
[26] M. Zhang, L.M. Dai, Nano Energy 1 (2012) 514–517.
[27] L.P. Zhang, Z.H. Xia, J. Phys. Chem. C 115 (2011) 11170–11176.
[28] J. Liang, Y. Jiao, J. Mietek, S.Z. Qiao, Angew. Chem. Int. Ed. 51 (2012) 1496–1500.
[29] S. Inamdar, H.S. Chio, P. Wang, M.Y. Song, J.S. Yu, Electrochem. Commun. 30 (2013) 9–12.
[30] D. Higgins, M.A. Hoque, M.H. Seo, R.Y. Wang, H. Fathy, Y.C. Ja, M. Pritzker, A.P. Yu, J.J. Zhang, Z.W. Chen, Adv. Funct. Mater. 24 (2014) 4325–4336.
[31] H. Wang, X.J. Bo, Y.F. Zhang, L.P. Guo, Electrochim. Acta 108 (2013) 404–411.
[32] S.Y. Gao, H.Y. Liu, K.R. Geng, X.J. Wei, Nano Energy 12 (2015) 785–793.

[33] C. Domínguez, F.J. Pérez-Alonso, S.A. Al-Thabaiti, S.N. Basahel, A.Y. Obtaid, A.O. Alyoubi, J.L.G. Fuente, S. Rojas, Electrochim. Acta 157 (2015) 158–165.
[34] Y.F. Li, M. Li, L.Q. Jiang, L. Lin, L.L. Cui, X.Q. He, Phys. Chem. Chem. Phys. 16 (2014) 23196–23205.
[35] D.Y. Zhao, J.L. Feng, Q.S. Huo, N. Melosh, G.H. Fredirckson, B.F. Chemlka, Science 279 (1998) 548–552.
[36] M. Kruk, M. Jaroniec, Chem. Mater. 12 (2000) 1961–1968.
[37] M. Imperor-Clerc, P. Davidson, A. Davidson, J. Am. Chem. Soc. 12 (2000) 11925–11933.
[38] G. Chen, Y. Liu, Y. Liu, Y. Tian, X. Zhao, J. Electroanal. Chem. 738 (2015) 100–107.
[39] Y.M. Liu, Y. Cao, N. Yi, W.L. Feng, W.L. Dai, S.R. Yan, H.Y. He, K.N. Fan, J. Catal. 224 (2004) 417–428.
[40] S.Q. Song, W.J. Zhou, Z.X. Liang, R. Cai, G.Q. Sun, Q. Xin, V. Stergiopoulos, P. Tsiakaras, Appl. Catal. B: Environ. 55 (2005) 65–72.